Part of the Special Issue: *Facets of Polymorphism in Crystals*

CRYSTAL GROWTH & DESIGN
2008
VOL. 8, NO. 1
44–56

Conformational Polymorphism in Oxybuprocaine Hydrochloride†

Ulrich J. Griesser,*,‡ Ram K. R. Jetti,‡ Mairi F. Haddow,‡ Thomas Brehmer,§ David C. Apperley,△ Andrew King,△ and Robin K. Harris△

Institute of Pharmacy, University of Innsbruck, Innrain 52, 6020 Innsbruck, Austria, Institute of Mineralogy and Crystallography, University of Vienna, Althanstrasse 14, 1090 Vienna, Austria, and Department of Chemistry, University of Durham, South Road, Durham DH1 3LE, United Kingdom

Received June 27, 2007; Revised Manuscript Received October 11, 2007

ABSTRACT: The structural and thermodynamic features of three polymorphic forms of the local anesthetic drug oxybuprocaine hydrochloride (OBPHC) were characterized by hot-stage microscopy, differential scanning calorimetry (DSC), pycnometry, Fourier transform infrared spectroscopy (FTIR), FT-Raman and solid-state NMR (SSNMR) spectroscopy as well as X-ray powder and single-crystal diffractometry. Mod II° crystallizes in the space group $P2_1/n$, is present in commercial products, and is the thermodynamically stable form at room temperature. Mod II° shows an endothermic transformation to mod I (mp 160 °C) at about 135 °C, indicating an enantiotropic relationship between these forms. Mod I (space group $I2/a$) shows a high kinetic stability and does not transform back to the more stable mod II° below the thermodynamic transition temperature (∼90 °C) on storage but does so in a solution-mediated process. Cooling mod I below −30 °C results in mod III ($P2_1/a$). This transition (T_{trs}: −33 °C) is highly reversible, proving the enantiotropic relationship between mod III and mod I. OBPHC is a classic example of conformational polymorphism demonstrating the interplay of molecular interaction forces and conformational flexibility. Two basic types of conformers can be found in the different polymorphs. Only one U-type conformer is present in the asymmetric unit of mod I, whereas in mod III two U-type conformers and in mod II° a type U- and an unusually bent type I conformer can be found. Computational modeling of the isolated molecule suggests that the I-type conformer is more stable than the U-type conformers.

1. Introduction

Crystal polymorphism is a widespread phenomenon in small organic molecules, which is defined by Grant[1] as the ability of a compound to crystallize in different crystalline phases with different arrangements and/or conformations of the molecules in the crystal lattice. Among drug compounds, rigid molecules are rather rare, and the vast majority of active pharmaceutical ingredients involve molecules with one to numerous rotatable bonds and molecular units with moderate to high conformational flexibility. The occurrence of multiple molecular conformations in different solid-state forms is referred to as "conformational polymorphism". This term as well as the structural and energetic aspects of this phenomenon have been extensively discussed by Bernstein,[2–4] and numerous representative examples of this type of crystal polymorphism have been reported (e.g., refs 5–13). Yu et al.[14] discussed some of the problems in the crystallization of conformationally flexible molecules highlighting a reduced crystallization tendency due to the potential presence of multiple conformers in the crystallization media. Probably the most prominent example of conformational polymorphism in pharmaceuticals is ritonavir.[15] The compound was first crystallized and manufactured as form I, which is the thermodynamically metastable (kinetic) form. Only after the production of 240 lots of Norvir capsules did the thermodynamically stable polymorph (form II) appear, whose solubility is much lower than that of form I (about one-fifth), which is why capsules containing this form failed the dissolution requirements. Although it was shown that form II contains an energetically less favorable conformation, the overall structure is energetically more stable, due to stronger hydrogen bonding. Moreover, the stable form II is also slightly less densely packed, which violates the density rule[16] and Kitaigorodsky's close packing principle[17] but highlights clearly that strong molecular interactions in crystals may overcome both packing efficiency and conformational energy. Another example that demonstrates the complex interplay of conformational freedom and intermolecular hydrogen bonding is indomethacin,[18] where the metastable α-form shows three different conformers in the asymmetric unit enabling the formation of a closer packed structure, whereas in the stable γ-form only one conformer is present. These and other examples make clear that conformational flexibility introduces interesting options for different molecular architectures in crystals but also adds an additional level of complexity in predicting crystal structures of practically relevant polymorphs.[19–21]

Oxybuprocaine hydrochloride (4-amino-3-butoxy benzoic acid-2-(diethylamino)ethylester monohydrochloride, OBPHC), a local anesthetic drug of the ester type (Figure 1), is a representative example for molecules with many conformational degrees of freedom. Besides the five and seven-membered sidechains with 11 rotatable bonds in total, the molecule shows the ability to form hydrogen bonds via the oxygen and chlorine atoms (acceptors) and the two amino groups (donor). Although the compound was synthesized in the early 1950s, the only indication of the existence of polymorphs can be found in the Pharmacopoeia Europoeia, which states simply, "It shows

† This is part 12 of a series of articles with the title "Polymorphic Drug Substances of the European Pharmacopoeia".

* Corresponding author. E-mail: ulrich.griesser@uibk.ac.at.
‡ University of Innsbruck.
§ University of Vienna.
△ University of Durham.

10.1021/cg070590d CCC: $40.75
Published on Web 01/02/2008

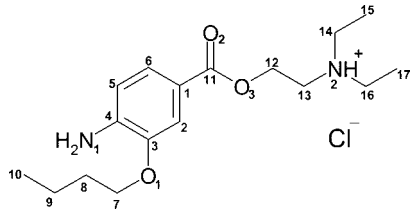

Figure 1. Molecular structure of oxybuprocaine HCl (OBPHC).

polymorphism". OBPHC is used as topical anesthetic, in ophthalmology (e.g., Benoxinate, Conjuncaine) and in otolaryngology (e.g., Novesine). Since the drug is exclusively applied as a diluted solution (1% or less), the existence of different solid-state forms is clearly not relevant for drug therapy. However, different polymorphs may exhibit distinct bulk properties and thus affect industrial production. Moreover, the knowledge of those forms which are durable under ambient conditions is also important for identity assays using solid sampling techniques such as IR-spectroscopy, a commonly applied identity test in pharmacopoeias.

In continuation of our work on solid-state properties of drug substances specified in the European pharmacopoeia,[22,23] the present study aims at a comprehensive understanding of the polymorphism of OBPHC, which represents one of the most intriguing local anesthetic drugs concerning its conformational flexibility. Besides single-crystal and powder X-ray diffraction methods, we also applied thermal analytical methods, polarized light microscopy, vibrational spectroscopy, and solid-state NMR (SSNMR) spectroscopy to characterize the structural and energetic features of existing crystal polymorphs. Details of sophisticated NMR experiments on mod II°, which assist in the assignment of resonances, have been published recently.[24] The crystal forms are named with Roman numerals. The modification which is thermodynamically stable at 20 °C is marked with a superscript zero.

2. Experimental Section

2.1. Materials. Three commercial batches of OBPHC, purchased from Gatt-Koller (K-Nr. 2186/0200 0800) and Agepha Wien (batch 670269 and batch 685830) were available and used without further purification. All solvents used in this study were p.a. quality.

2.2. Hot-Stage Microscopy. Thermomicroscopic investigations were performed with a Reichert Thermovar polarization microscope (Reichert, Vienna, A) equipped with a Kofler hot stage (Reichert, Vienna, A) and a Linkam stage LTS 350 connected to a TP92 temperature controller and a LNP 1 liquid nitrogen pump (Linkam Scientific Instruments Ltd., Tadworth, Surrey, UK). The microscopic images were recorded with a DP50 digital camera attached to an Olympus BX-50 microscope (Olympus Optical GmbH, Vienna, A).

2.3. Differential Scanning Calorimetry (DSC). DSC measurements were performed with a DSC 7 system (Perkin-Elmer, Norwalk, Ct., USA) using the Pyris 2.0 software. Samples of approximately 2 ± 0.0005 mg (using a UM3 ultramicrobalance, Mettler, Greifensee, CH) were weighed into Al-Pans (25 μL). Dry nitrogen was used as the purge gas (purge: 20 mL min^{-1}). The temperature calibration was performed with pure benzophenone (mp 48.0 °C) and caffeine (mp 236.2 °C) and energy calibration with pure indium (purity 99.999%, mp 156.6 °C, $\Delta_{fus}H$: 28.45 J g^{-1}). Low-temperature DSC thermograms were recorded with a Perkin-Elmer DSC7 equipped with a CCA-7 controlled cooling device (Perkin-Elmer, Norwalk, Ct., USA). The runs were recorded at a head temperature of −80 °C and for calibration n-decane (−28 °C), water (0 °C), and indium 99.999% was used.

2.4. Infrared Spectroscopy. Fourier transform infrared (FTIR) spectra were recorded with a Bruker IFS 25 spectrometer (Bruker Optik GmbH, Ettlingen, D). Samples were scanned as potassium bromide

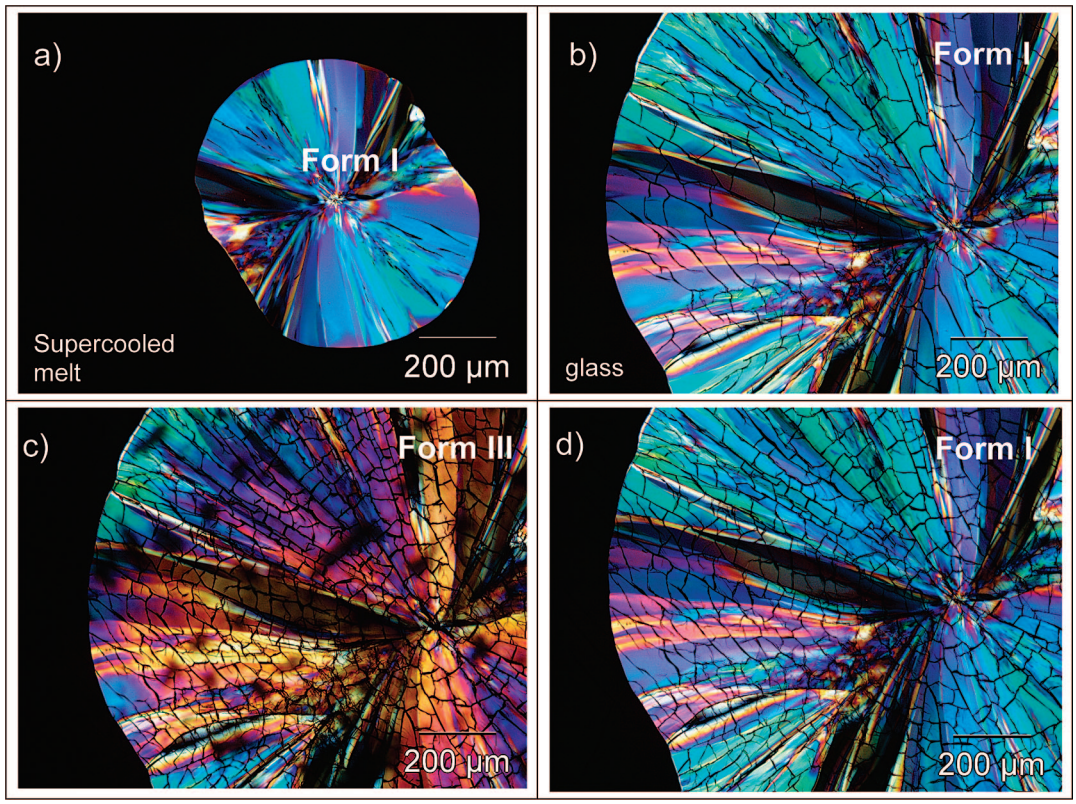

Figure 2. Polarized light microphotographs of OBPHC melt film preparations; (a) nucleation and growth of mod I from the melt, $T = +90$ °C; (b) $T = +10$ °C, growth of the mod I spherulite terminated, formation of cracks; (c) cooled to −70 °C, mod III (blurred dark spots derive from the crystallization of ice on top of the coverslip); (d) reheated to +35 °C, mod I.

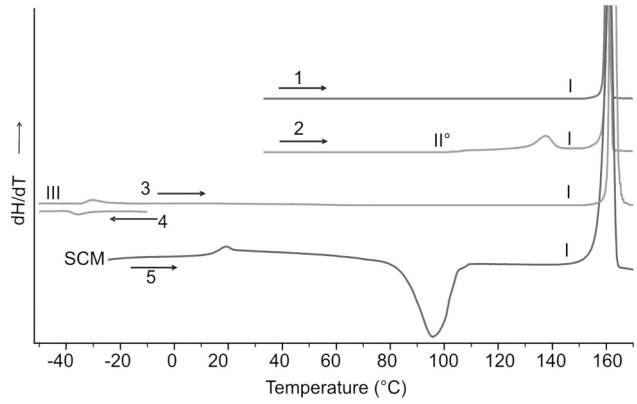

Figure 3. DSC curves of OBPHC polymorphs. (1) mod I; (2) mod II°; (3) mod III; (4) cooling curve of mod I; (5) supercooled melt (SCM) on heating, showing a glass transition and the crystallization to mod I. Heating and cooling rates: 5 K min^{-1}.

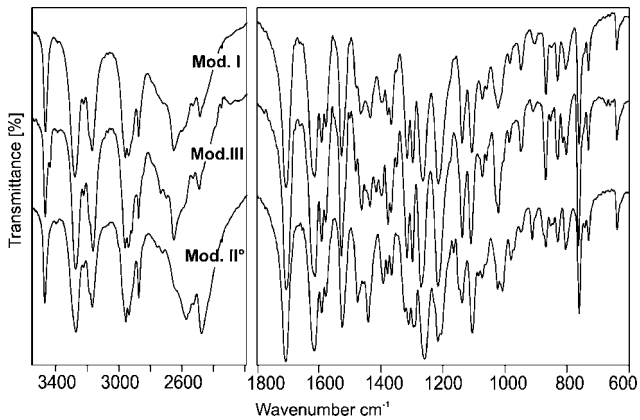

Figure 4. FTIR spectra of OBPHC polymorphs. The spectra of mods II° and I were recorded at 20 °C, form III at about −50 °C, (KBr disk).

disks over a range of 4000 to 600 cm^{-1} at an instrument resolution of 2 cm^{-1} (100 scans per spectrum). Approximately 2 mg of OBPHC was used per 300 mg of KBr. The variable temperature conditions were adjusted with a SPECAC (Graseby Specac Limited., Orpington, UK) variable temperature cell (P/N 21525) with a temperature control unit (P/N 20120). For low temperature experiments, the temperature cell was sealed with NaCl Vacuum Jacket windows, and the chamber was evacuated with a vacuum pump (200 mbar). Liquid nitrogen was used as the refrigerant.

2.5. Raman Spectroscopy. The Raman spectra were recorded with a Bruker RFS 100 Raman spectrometer (Bruker Optik GmbH, Ettlingen, D), equipped with a NIR laser (Nd:YAG, 1064 nm) as excitation source and a liquid-nitrogen-cooled, high-sensitivity Ge-detector. Samples were packed into small aluminum cups, and the spectra were recorded with a laser output power of 300 mW and instrument resolution of 4 cm^{-1} (64 scans per spectrum). The variable temperature conditions were adjusted with the variable temperature cell (SPECAC) as described above (IR spectroscopy) using the respective Raman accessories. The samples were recorded in aluminum cups, and for the adjustment of subambient temperatures the cell was evacuated (200 mbar) and cooled with liquid nitrogen.

2.6. Solid-State NMR Spectroscopy. Carbon-13 and nitrogen-15 cross-polarization magic-angle spinning (CPMAS) spectra were obtained at 75.43 and 30.40 MHz, respectively, using a Varian Unity Inova spectrometer based on a 7.05 T Oxford Instruments superconducting magnet. The probe accepts 7 mm o.d. (outside diameter) zirconia rotors, which were fitted with Kel-F end-caps. A flip-back procedure was implemented. Proton decoupling at a power equivalent to a frequency of ca. 60 kHz was employed during acquisition. The MAS rates were usually between 4 and 5 kHz for ^{13}C and were 4.25 kHz for ^{15}N. Contact times were normally 3 ms for ^{13}C and 10 ms for

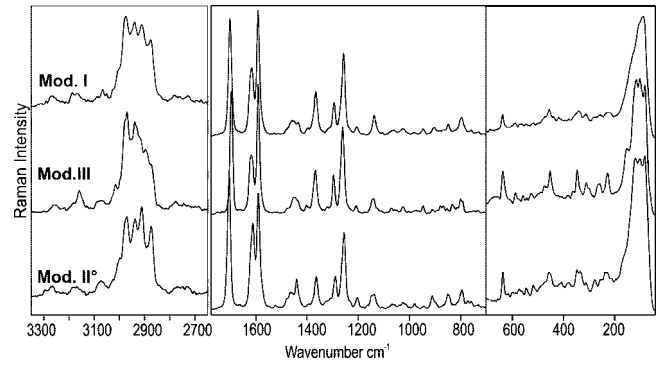

Figure 5. Raman spectra of OBPHC modifications. The spectra of mods I and II° were recorded at 25 °C, mod III at −40 °C. The intensity scales of the spectral windows 3400 to 2650 and 700 to 50 cm^{-1} are multiplied in relation to the one in the center (1700 to 700 cm^{-1}) for visualization reasons.

^{15}N. The numbers of transients were generally between 200 and 800 for ^{13}C but between 30 000 and 40 000 for ^{15}N. Recycle delays were 1 or 2 s. The dipolar dephasing pulse sequence[26] was employed to identify quaternary and methyl carbon signals and the $^{15}NH_2$ resonance, with decoupling windows of 40 μs for ^{13}C and 200 μs for ^{15}N. Variable-temperature ^{13}C spectra were acquired between ambient (23 °C) and a nominal −90 °C using a stream of cooled nitrogen gas. Calibration shows that the nominal temperatures are close (within 2 K) to the true sample temperatures.

High-speed (30 kHz) MAS proton spectra were obtained at 499.75 MHz using a Varian Infinity Plus 500 spectrometer fitted with a probe accepting 2.5 mm zirconia rotors (with Torlon spacers and drive-tips). For each spectrum 32 transients were acquired, each following a 90° pulse of duration 3 μs.

Chemical shifts are quoted with respect to the signals for solution-state tetramethylsilane (for ^1H and ^{13}C) or nitromethane (for ^{15}N) but were recorded using samples of poly(dimethylsiloxane) (^1H; $\delta_H = 0.1$ ppm), solid adamantane (^{13}C; high frequency line at $\delta_C = 38.4$ ppm) and solid ammonium nitrate (^{15}N; NO_3 peak at $\delta_N = -5.1$ ppm).

2.7. X-Ray Powder Diffractometry (XRPD). The powder X-ray diffraction patterns were obtained using a Siemens D-5000 diffractometer (Bruker-AXS, Karlsruhe, Germany) equipped with a theta/theta goniometer, a Goebel mirror, a 0.15° soller slit collimator and a scintillation counter. The patterns were recorded at a tube voltage of 40 kV and a tube current of 35 mA, applying a scan rate of 0.005° 2θ s^{-1} in the angular range of 2 to 40° in 2θ. Temperature-controlled experiments were performed with a low-temperature camera TTK (Anton Paar KG, Graz, A). The program PowderCell for windows[27] was used for the calculation of the theoretical powder patterns from single crystal data.

2.8. X-ray Data Collection and Crystal Structure Determinations. The X-ray data for modifications I, II° (RT), II° (LT), and III were collected on a Nonius Kappa-CCD diffractometer using Mo Kα radiation with a crystal to detector distance of 35 mm except for mod II° (RT) where the distance was 40 mm. The intensity data for all the structures mod I/mod II°/mod II° 200K/ mod III 200K were collected using 169/147/351/333 CCD-frames with a phi-increment of 2/2/1/1 degrees and a counting time of 120/40/40/120 s per frame. All the four structures were solved by direct methods, using the program SIR92,[28] and refinements were carried out using the SHELXTL (version 6.12) program package.[29] In the case of mod I structure, the alternative setting for the space group *I2/a* has been checked and can be transformed to *C2/c*. All the H atom positions in I−III were generated by a riding model on idealized geometries with $U_{iso}(H) = 1.2U_{eq}(C)$ for phenyl C−H and $U_{iso}(H) = 1.5U_{eq}(C)$ for CH_3 groups and were refined isotropically. However, the positions of the H atoms bound to NH_2 groups were located in difference Fourier maps, and these H-atoms were also refined as riding, with $U_{iso}(H) = 1.2U_{eq}(N)$, while the H atoms bound to tertiary ammonium (+N−H) groups were located in difference Fourier maps and refined isotropically without any constraints. The side-chain carbon atoms C(9), C(10), C(14), and C(17) in mod I and C(8), C(8′), C(9), C(9′), C(10), and C(10′) in mod II° were disordered over two sites with occupancies in the ratio 0.65:0.35, 0.30:0.70, 0.65:

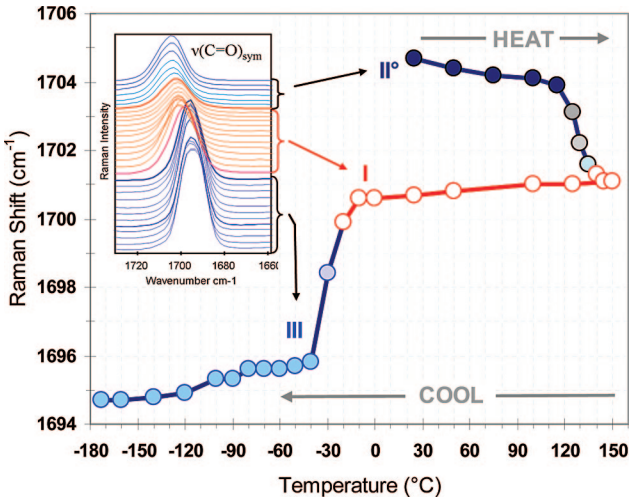

Figure 6. Variable temperature Raman experiment of OBPHC; plot of the carbonyl band wavenumbers (cm^{-1}), taken from the peak maxima (inset), versus temperature. Heating cycle 25−150 °C followed by a cooling cycle down to −173 °C.

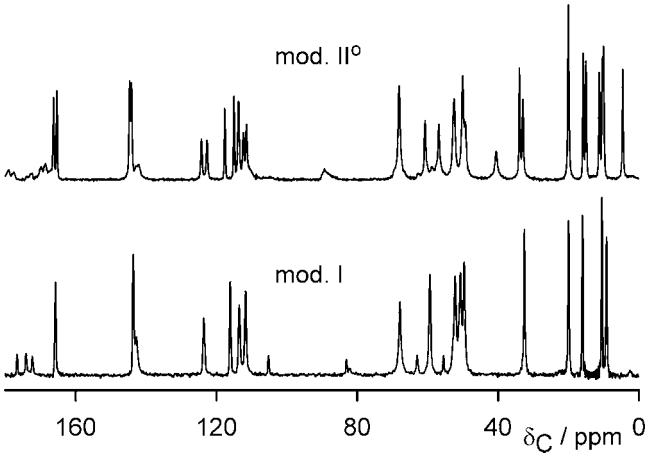

Figure 7. Solid-state ^{13}C NMR-spectra of OBPHC modifications. Mod I and II° recorded at room temperature.

0.35, 0.75:0.25 for mod I and 0.90:0.10, 0.60:0.40, 0.90:0.10, 0.65:0.35, 0.65:0.35, 0.65:0.35, respectively, for mod II. Also the chloride Cl(1) ions in mod III are disordered over two sites with occupancies in the ratio 0.90:0.10. In the case of mod I, the *U*-values seem to be a bit too large, and this is because of poor crystal quality. Further details of the refinement are collected in Table 1. Molecular graphics were generated using the program XP, an in-built program of SHELXTL suite.[29] The crystallographic data of the modifications I-III have been deposited with the Cambridge Crystallographic Data Centre, CCDC Nos. 651280 (mod I), 651281 (mod II, RT), 651282 (mod II, LT), 651283 (mod III).

2.9. Molecular Modeling. To gauge which is the most stable molecular conformation without crystal packing influences and charges, computational modeling of OBPHC was performed using MacroModel as inmplemented in Maestro V7.5.[30] Starting geometries for the five independent molecules in the three crystal structures were taken directly from the crystal structures of the hydrochloride salt and modified to produce the neutral molecule. The molecules that show disorder are modeled using the different confromations present in the disorder. This resulted in 14 molecular conformations whose important torsion angles are given in the Supporting Information. The force field used to compare energies was MMFF94s. The Merck Molecular Force Field, which was developed for medium-sized organic compounds, and in particular drug molecules, has been found to be consistently good in predicting conformational energy differences for a range of organic molecules, when tested by its developers[36] but also independently.[37] Conformational searching was performed using the force field MMFF94x (as implemented in MOE),[31] with a maximum of 10 000 starting structures.

3. Results and Discussion

3.1. Preparation of the Polymorphs. Mod II° is the thermodynamically stable form at room temperature and was present in the available commercial products. This form crystallizes from apolar solvents, such as *n*-hexane or toluene, and also from ethanol. Single crystals of this form, suitable for crystal structure determination, were obtained from an ethanol solution by vapor diffusion with diethylether.

Mod I can be simply obtained by heating mod II° above 140 °C or by crystallization from hot saturated water, methanol, acetone, dioxane, or ethylacetate solutions. Single crystals for crystal structure determination were obtained by slowly cooling a saturated ethylacetate-solution.

Mod III is formed by cooling mod I to below −30 °C. The spontaneous solid–solid transformation occurs between −25 and −30 °C and is reversible, which is why this low temperature form cannot be maintained at any temperature above −25 °C.

3.2. Thermal Analysis. 3.2.1. Hot-Stage Microscopy. The commercial product consists of small, highly birefringent prismatic crystals and aggregates of mod II°. On heating, a transformation to the high temperature form mod I occurs at about 135 °C. This process is indicated by a darkening of the crystals and the formation of a secondary pattern within the crystals, whose outer shape is maintained (pseudomorphosis, see Supporting Information). At about 140 °C, the compound starts to sublime, and the deposition of needles of mod I and condensation droplets on the coverslip can be observed. The equilibrium melting point of mod I can be established at 160 °C. On slow cooling of the melt, mod I nucleates and grows to spherulites (Figure 2a). The maximal crystal growth rate of mod I is estimated to occur at roughly 100 °C. At about 30 °C, the growth stops, and below the glass transition temperature (about 15 °C) cracks appear (Figure 2b). On further cooling, mod I transforms to a low-temperature form (mod III) at about −35 °C, which is only indicated by a change in the interference colors (Figure 2c). Reheating to −25 °C shows the recurrence of the original interference colors (Figure 2d) due to the retransformation to mod I. This transformation is highly reversible, indicating an enantiotropic relationship between mod III and mod I. Interestingly, the stable mod II° does not nucleate in the melt at all, and seeding experiments at about 60 °C showed that also the crystal growth rate of mod II° in the supercooled melt is extremely low. Furthermore, no retransformation of mod I to mod II° could be observed on cooling, which lets us assume from the hot-stage microscopy experiments that, in the case of enantiotropism between these forms, the transformation is either kinetically hampered or that the observed transformation of mod II° to form I is monotropic.

3.2.2. Differential Scanning Calorimetry. The DSC curve of mod I (Figure 3, curve 1) shows only a single melting endotherm at 159.9 °C ($\Delta_{fus}H_I$: 35.5 kJ mol^{-1}). The phase transition of mod II° to mod I is recorded as an endothermic process ($\Delta_{trs}H_{II°\text{-}I}$: 5.4 kJ mol^{-1}) at 135 °C. (Figure 3, curve 2). On cooling samples of mod I, an exothermic peak at −35 °C (Figure 3, curve 4) can be observed, indicating the phase transformation to mod III ($\Delta_{trs}H_{I\text{-}III}$: −0.4 kJ/mol). An endothermic peak at about −31 °C ($\Delta_{trs}H_{III\text{-}I}$: +0.4 ± 0.2 kJ/mol) in the heating curve (Figure 3, curve 3) confirms that the transformation between mod III and mod I is reversible. These data coincide very well with the hot-stage microscopy observations and beyond that, from the fact that the transition of mod II° to mod I is

Table 1. Summary of Crystallographic Data and Structure Refinement Parameters for Oxybuprocaine Hydrochloride Polymorphs I, II°, and III

compound	mod I	mod II° (RT)	mod II° (LT)	mod III
molecular formula	$C_{17}H_{29}O_3N_2Cl$	$C_{17}H_{29}O_3N_2Cl$	$C_{17}H_{29}O_3N_2Cl$	$C_{17}H_{29}O_3N_2Cl$
M_r	344.87	344.87	344.87	344.87
crystal system	monoclinic	monoclinic	monoclinic	monoclinic
space group	*I*2/*a*	*P*2$_1$/*n*	*P*2$_1$/*n*	*P*2$_1$/*a*
a (Å)	14.416(3)	12.2207(4)	12.2420(2)	14.1880(3)
b (Å)	11.992(2)	24.3124(9)	24.0071(4)	11.6570(2)
c (Å)	22.632(5)	14.2109(5)	14.1575(2)	22.5140(4)
α (deg)	90	90	90	90
β (deg)	91.63(3)	113.510(2)	113.865(1)	92.109(2)
γ (deg)	90	90	90	90
V (Å^3)	3911.0(14)	3871.78(19)	3805.07(10)	3721.06(12)
Z	8	8	8	8
T (K)	293(2)	293(2)	200(2)	200(2)
D_{calc} (g cm^{-3})	1.171	1.183	1.204	1.231
absorption coefficient (mm^{-1})	0.210	0.212	0.216	0.221
F (000)	1488	1488	1488	1488
color, habit	colorless prism	colorless plate	colorless plate	colorless prism
crystal size (mm)	0.25 × 0.25 × 0.20	0.30 × 0.30 × 0.30	0.30 × 0.30 × 0.30	0.25 × 0.25 × 0.20
θ range for data collection (deg)	1.92–25.02	2.47–25.03	1.70–25.01	2.26–25.03
index ranges	$-17 < h < 17$, $-14 < k < 13$, $-26 < l < 26$	$-14 < h < 14$, $-28 < k < 28$, $-16 < l < 16$	$-14 < h < 14$, $-26 < k < 28$, $-16 < l < 16$	$0 < h < 16$, $0 < k < 13$, $-26 < l < 26$
reflections collected	6308	12828	12348	12647
independent reflections	3446 (R_{int} = 0.0327)	6749 (R_{int} = 0.0366)	6704 (R_{int} = 0.0208)	6568 (R_{int} = 0.0269)
reflections with $I > 2\sigma(I)$	1691	3754	4973	4925
data/restraints/parameters	3446/0/239	6749/0/476	6704/0/458	6568/0/597
goodness-of-fit on F^2	1.018	1.036	1.039	1.032
final *R* indices [$I > 2\sigma(I)$]	R_1 = 0.0822, wR_2 = 0. 2260	R_1 = 0.0619, wR_2 = 0.1606	R_1 = 0.0457, wR_2 = 0.1161	R_1 = 0.0421, wR_2 = 0.0973
R indices (all data)	R_1 = 0.1639, wR_2 = 0.2732	R_1 = 0.1265, wR_2 = 0.1902	R_1 = 0.0684, wR_2 = 0.1279	R_1 = 0.0657, wR_2 = 0.1070
largest difference peak and hole, e Å^{-3}	0.294/−0.216	0.439/−0.316	0.496/−0.248	0.346/−0.210
type of molecule (conformer)	only type U	mixture of type U and I	mixture of type U and I	only type U, but two conformers

endothermic, we can clearly attest that these forms are enantiotropically related (heat of transition rule[16]). It is in fact surprising that the high-temperature form (mod I) transforms to mod III on cooling and not to mod II°, although the latter is thermodynamically more stable below the transition point of II° ↔ I, as will be discussed in more detail below.

The DSC curve of the quench-cooled melt shows a glass transition at about 15 °C with an excess endotherm, followed by an endothermic reaction between 80 and 100 °C, indicating the crystallization of mod I from the supercooled melt. The ratio of the glass transition temperature (T_g) and the melting point of mod I ($T_{fus,I}$) in Kelvin is 0.67 and lies well within the predictable range (0.7 ± 0.05)[32,33] for small organic molecules.

3.3. FTIR and Raman Spectroscopy. Both FTIR (Figure 4) and Raman spectra (Figure 5) allow a clear identification of the individual polymorphs. The differences concern almost all molecular vibration modes including ring and ether functions, and of course those that are expected to be involved in strong or weak hydrogen bonding (amino, carbonyl functions) or are affected by conformational changes (alkyl chains). The *ν* N−H stretching vibration (IR) of the forms lie within a few wavenumbers (see Table 5), indicating a similar strength in the hydrogen bonding of the primary amino group. On the other hand, the protonated tertiary amine (R_3N^+H) bands (IR: ∼2700–2400 cm^{-1}) of mod II° display quite different intensities to those of the two other forms. This difference can obviously be ascribed to a difference in the $N^+H\cdots Cl^-$ interaction in mod II°. Also the differences in the low energy motion bands of the Raman spectra (far-infrared region below 200 cm^{-1}) indicate, that the three forms represent three distinct materials with dissimilar intramolecular interactions. To monitor the transitions and temperature-dependent changes with IR- and Raman spectroscopy, mod II° was heated in 5−20 °C steps from 20 to 150 °C and down to −173 °C. Figure 6 shows as an example the changes and temperature-dependent wavenumber-shifts of the C═O band. The band undergoes a bathochromic shift of 10 cm^{-1} in this temperature scan, and the observed steps clearly show the phase transition of mod II° to I between 120 and 140 °C and the transition of mod I to III between −20 and −40 °C. It is striking that a further, albeit small, but rather discontinuous bandshift can be recognized below −80 °C. This probably indicates a discontinuous decrease in mobility and motion of the sidechains, which can be also seen from the increase of band intensities or band splittings when decreasing the temperature.

3.4. Solid-State NMR Spectroscopy. CPMAS ^{13}C spectra of mod I and II°, obtained at ambient probe temperature, are shown in Figure 7, and the chemical shift data are given in Table 2. Such spectra give immediate information about the number of molecules in the crystallographic asymmetric unit. In the case of mod I, the number of resonances is equal to the number of carbon atoms in the molecule, so it can be concluded that the asymmetric unit is one molecule. Note that the two ethyl groups of the dimethylamino unit give four signals and are thus shown to be nonequivalent cyrstallographically, although in the solution state they would give two peaks only. In contrast to mod I, the spectrum of mod II° contains doublets for most of the carbon atoms, so it is clear that there are, in this case, two molecules in the asymmetric unit. These conclusions are, of course, confirmed by the diffraction experiments (see below). The assignment of the signals listed in Table 2 has been carried out (a) from known ranges for chemical groupings, (b)

Table 2. Carbon-13 Chemical Shifts and Assignments for OBPHC

carbon type[a]	carbon number	database shift (ppm)	solution-state[b] shift (ppm)	mod I shift (ppm)	solution-to-solid change[c] (ppm)	mod II° shift (ppm)[d]	splitting for mod II° (ppm)
C═O (Q)	C-11	165.9	166.30	165.9	−0.4	166.3	0.9
						165.4	
C−O (Q)	C-3	146.8	145.69	143.9	−1.8	144.6	0.5
						144.1	
C−N (Q)	C-4	135.7	142.63	143.1	0.5	144.1	1.9
						142.2	
CH	C-6	130.6	124.40	123.8	−0.6	124.2	1.5
						122.7	
C−C═O (Q)	C-1	128.7	117.51	116.3	−1.2	117.6	2.7
						114.9	
CH	C-5	122.6	113.17	113.8	0.6	112.3	0.9
						111.4	
CH	C-2	110.4	112.12	111.9	−0.2	113.6	<0.3
H_2C−O	C-7	67.9	68.40	68.1	−0.3	68.0	<0.3
H_2C−O	C-12	62.9	58.35	59.5	1.1	60.9	4.2
						56.7	
H_2C−N	C-13	51.5	49.87	52.4	2.5	52.6	2.6
						50.0	
H_2C−N	C-14/16	47.9	47.58	50.8	3.2	52.6	
				49.9	2.3	50.0	
						49.3	
						40.5	
CH_2	C-8	31.7	31.44	32.6	1.2	33.9	1.0
						32.9	
CH_2	C-9	19.2	19.50	20.1	0.6	20.0	<0.3
CH_3	C-10	13.8	14.09	16.1	2.0	15.8	0.8
						15.0	
CH_3	C-15/17	11.4	9.00	10.6	1.6	11.2	
				9.4	0.4	10.3	
						10.1	
						4.6	

[a] Q indicates a quaternary carbon (signal picked out by dipolar dephasing experiments; see the Supporting Information). [b] In $CDCl_3$. [c] Mod I minus solution state. [d] For a detailed discussion of the assignments of mod II°, see ref 24. [e] These splitting magnitudes are incorrectly transposed in ref 24.

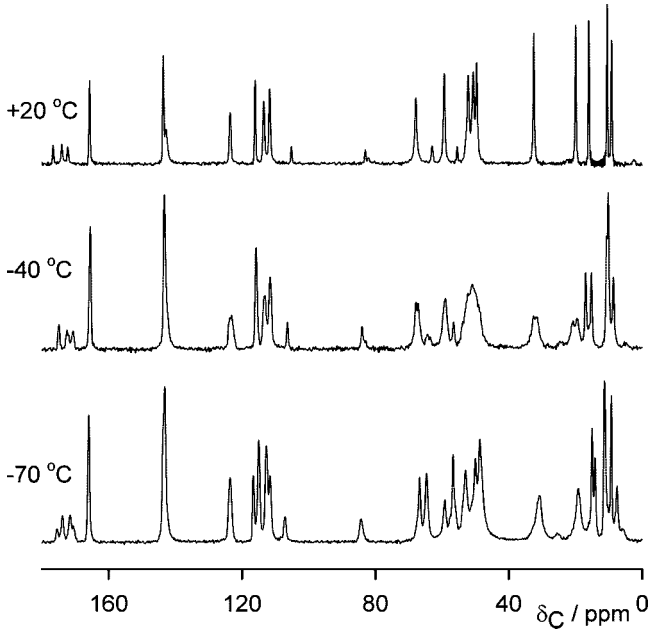

Figure 8. Solid-state ^{13}C NMR spectra of OBPHC mod I (20 °C) and mod III (−40 and −70 °C).

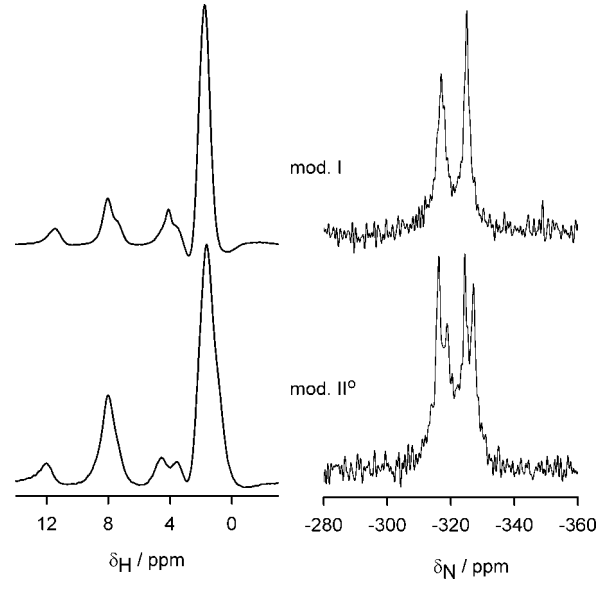

Figure 9. Solid-state ^{1}H (left) and ^{15}N NMR spectra (right) of OBPHC mods I and II°. Both were recorded at ambient probe temperature.

by use of the chemical database service at Daresbury, UK (Table 2, column 3), (c) from comparison of solution-state and solid-state data, (d) using dipolar dephasing experiments, which distinguish quaternary and methyl carbon signals from those for CH and CH_2 carbons (see Supporting Information), (e) from line-broadening arising from residual dipolar coupling to the quadrupolar ^{14}N nucleus (which identifies signals for carbons directly bonded to nitrogen), and, finally, (f) for mod II° from detailed two-dimensional (2D) experiments and shielding computations.[24] There are minor residual uncertainties for a small number of the signals for mod II°. The database values, which relate to solution-state spectra, are given in Table 2. Whereas some of these chemical shifts differ substantially (by up to 9 ppm) from the observed solution-state values, the frequency order of the signals does not appear to be in doubt.

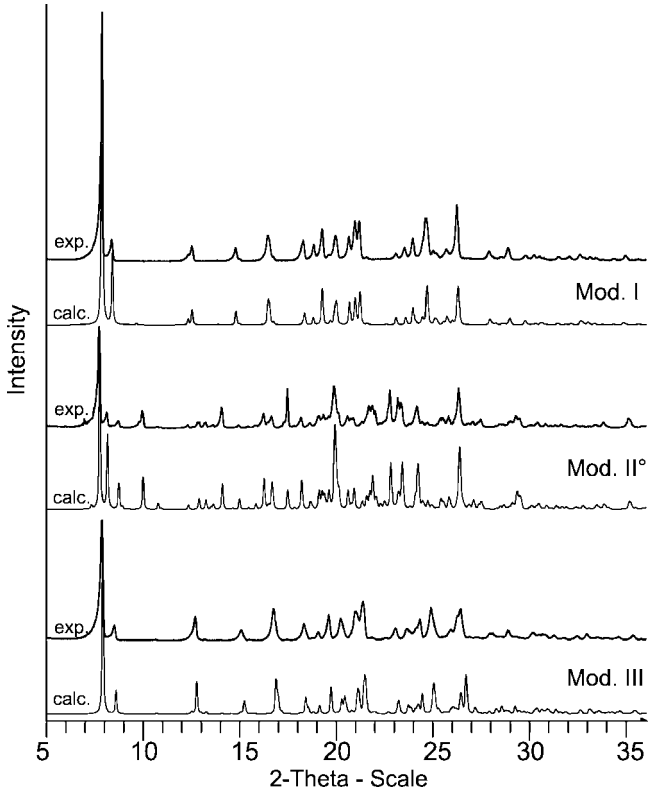

Figure 10. Experimental (exp.) and calculated (calc.) powder X-ray diffraction patterns of the three polymorphs of OBPHC. Mods I and II° were recorded at room temperature, mod III at −40 °C.

Chemical shifts for the solution state (in chloroform) are given in Table 2, along with values for the solution-to-solid (mod I) changes in shifts. It can be seen that, whereas some of the aromatic carbon signals move to low frequency on crystallization to mod I, all resonances for the aliphatic carbons (except C7) move to high frequency (several of them by 2 ppm or more). We attribute these changes to the fixing of conformations in the solid as compared to the flexibility accorded to the solution state.[25]

The spectrum for mod II° shows two signals (at 40.5 and 4.6 ppm) which are in spectral regions clear of signals for mod I. We have shown[24] by 2D INADEQUATE spectra that the carbons in question are bonded and that they correspond to an ethyl group. We have traced their unusual chemical shifts to conformational effects originating in the I-conformer (present in mod II° only). Specifically, these signals arise from carbons that have two gamma-*gauche* carbon neighbors, a result of the bent conformation of the I-conformer (see below).

The dipolar dephasing experiments,[26] which used a dephasing interval of 40 μs, showed strong residual signals from C8 and C9 for both polymorphs, though for mod II° only one of the C9 signals was resolved. This shows that the propyl end of the butoxy side-chain has substantial mobility. For mod I, the two CH_2 peaks of the diethylamino group also showed a (smaller) residual signal, indicating some mobility in this region also, but this was less evident for mod II°.

At the magnetic field used, the signals for C13, C14, and C16 are not noticeably broadened by residual dipolar coupling to nitrogen, but this effect is marked for C4, indicating a considerable difference in the strength of the quadrupolar interaction at the two different ^{14}N nuclei. The magnitudes of the crystallographic splittings for mod II° (Table 2) vary widely since precise chemical shifts are very sensitive to both the molecular geometry and the intermolecular environment. The putative splittings cannot be resolved for C5, C9, C14, and C16, and in these cases the chemical shifts are within 0.1 ppm of the corresponding values for mod I. Given that the conformation of one of the mod II° molecules is similar to that in mod I, one might expect that one member of each doublet for mod II° would have a very similar chemical shift to that of mod I. The fact that this is obviously not true shows that the intermolecular effects on the shifts are comparable to conformational influences. However, the biggest mod II° splittings are for C1 and C8, which are adjacent to the carboxyl group, suggesting that conformational effects dominate for these carbons.

As the probe temperature is lowered (in ca. 10 K steps) from ambient, the ^{13}C spectrum of mod I shows a remarkable series of changes (Figure 8), which start already at 0 °C and continue to the lowest temperature investigated (−90 °C). A more

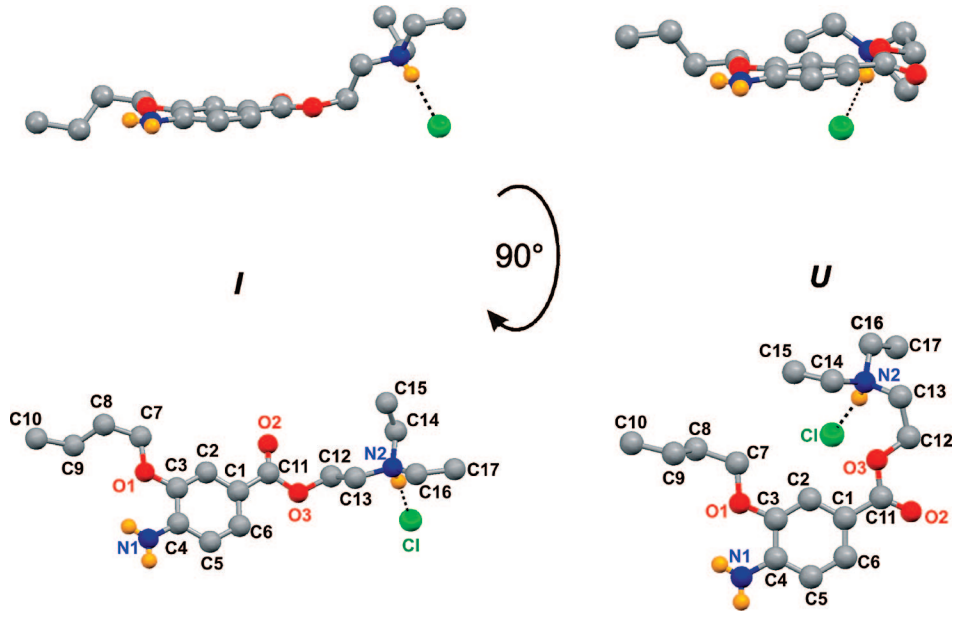

Figure 11. The two types of conformations in the OBPHC modifications **I**–**III**; linear (type **I**) and a bent type (type **U**).

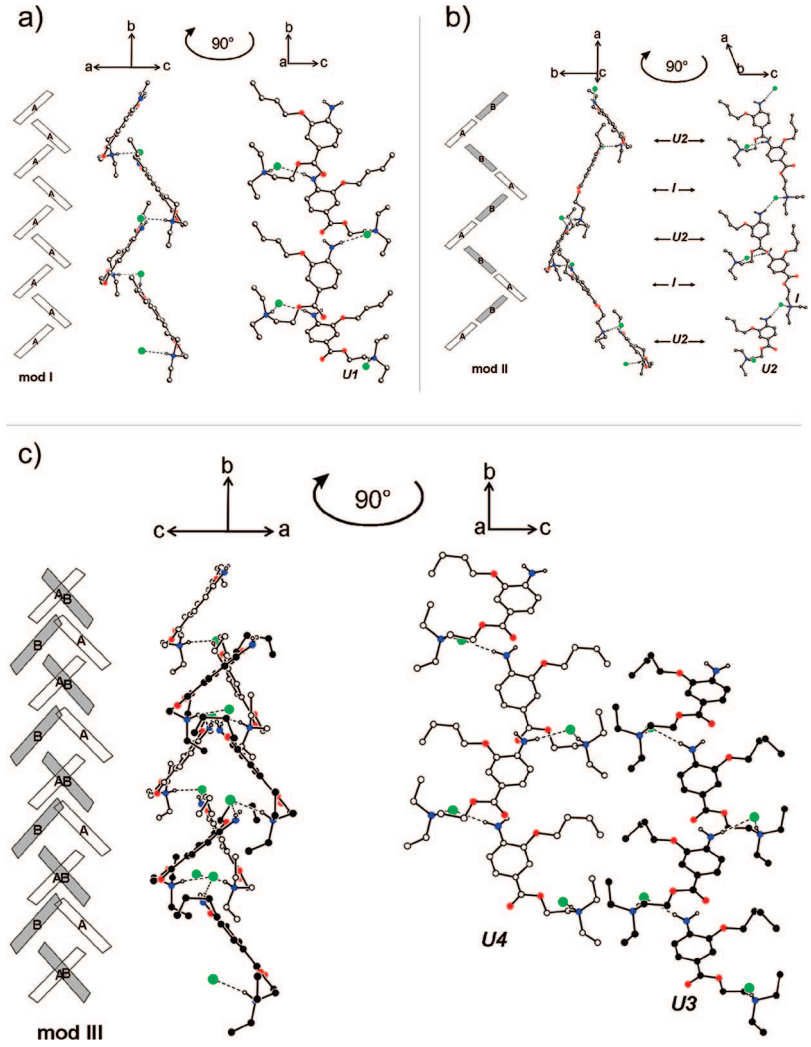

Figure 12. Packing schemes of the molecule types **U** and **I** in the crystals of mod **I** (a), mod **II**° (b), and mod **III** (c). H atoms of the phenyl and alkyl groups are omitted for clarity. The $NH_2\cdots Cl^-$ and $N^+H\cdots Cl^-$ contacts are drawn as dotted lines. **U1**−**U4**: four different conformers of type **U**. **A** and **B** denote the molecules in the asymmetric unit.

complete set of variable-temperature spectra is included in the Supporting Information. Whereas a detailed understanding of these variations is not yet available, it is likely that there are two intermingled causes: (a) the transition from mod I to mod III, with the accompanying increase in the size of the asymmetric unit, and (b) interplay of mobility of parts of the sidechains with either the MAS frequency or the frequency equivalent of the decoupler power (ca. 60 kHz). The former effect should result in splittings, while the latter causes line broadening (and accompanying loss of peak height). In addition, it is always likely that some resonances have intrinsically temperature-dependent chemical shifts. At modestly lowered temperatures (even beginning to be apparent at 0 °C), some of the aliphatic lines are broadened and lose peak height. The first clear splitting (of the C10 resonance) occurs at −30 °C, indicating that the mod I → mod III transformation has occurred. Other splittings appear to develop later. The aliphatic (side-chain) region is affected far more significantly than the aromatic and carboxyl region. The only substantial changes in the latter are (a) the appearance of four peaks in the C1/C5/*C*2 band at −50 °C and below, and (b) the apparent sharp reduction of the C4 line width at −90 °C (alternatively explicable as a splitting of the C3 signal). A detailed assignment of the peaks in the mod III spectrum is not feasible at this time, but the variations with temperature confirm the existence of substantial mobility in the side-chains.

The spectrum of mod II° does not change significantly as the temperature is lowered to −50 °C, reinforcing the conclusions about transformations obtained from thermochemical methods.

Nitrogen-15 CPMAS spectra of mods I and II° are shown in Figure 9. The spectrum of mod I contains two clear signals (δ_N = −317.1 and −325.8 ppm), whereas four (δ_N = 316.3, −319.0, −324.5, and −327.2 ppm) are seen for mod II°, as expected from the asymmetric units involved. The NH_2 resonance or resonances were identified as those to high frequency by dipolar dephasing experiments.[26]

Figure 9 also illustrates fast MAS proton spectra of mods I and II°. These show separate regions of resonances for aliphatic and aromatic protons plus high-frequency signals for the hydrogen bonds at chemical shifts δ_H = 11.1 and 11.8 ppm for mods I and II°, respectively. These values suggest that on average the hydrogen bonds in mod II° are slightly stronger than those in mod I, which, while it is in accord with the low-temperature stability of mod II°, is not evident in the results from X-ray diffraction (see below).

Table 3. Geometrical Parameters for Hydrogen Bridges[a] in Oxybuprocaine Hydrochloride Polymorphs I, II°, and III

compound	interaction	H···A (*d*, Å)	D···A (D, Å)	D−H−A (*θ*, °)
mod I	$N^+H\cdots Cl^-$	2.14	3.07	152
	$NH_2\cdots Cl^-$	2.27	3.27	170
	intra $NH_2\cdots O$	2.27	2.64	100
	$C(14)H\cdots Cl^-$	2.64	3.72	178
mod II° (LT)	$N^+H\cdots Cl^-$	2.05	3.06	175
	$NH_2\cdots Cl^-$	2.28	3.28	169
	intra $NH_2\cdots Cl^-$	2.07	3.05	165
	$NH_2\cdots Cl^-$	2.40	3.34	155
	intra $NH_2\cdots O$	2.26	2.63	100
	$C(14)H\cdots Cl^-$	2.57	3.58	155
	$C(14)H\cdots Cl^-$	2.60	3.66	167
	$C(16)H\cdots O$	2.16	3.21	163
	$C(16)H\cdots Cl^-$	2.68	3.64	147
mod III	$N^+H\cdots Cl^-$	2.14	3.08	154
	$NH_2\cdots Cl^-$	2.24	3.24	172
	intra $NH_2\cdots O$	2.23	2.63	102
	$N^+H\cdots Cl^-$	2.13	3.10	161
	$NH_2\cdots Cl^-$	2.31	3.31	171
	intra $NH_2\cdots O$	2.22	2.65	104
	$C(14)H\cdots Cl^-$	2.77	3.60	134
	$C(16)H\cdots O^-$	2.24	3.28	160
	$C(17)H\cdots O$	2.40	3.28	138
	$C(17)H\cdots Cl^-$	2.73	3.60	137

[a] All O−H, N−H, and C−H distances are neutron normalized to 0.983, 1.009, and 1.083 Å. $\pi\cdots\pi$ corresponds to aryl···aryl perpendicular distances calculated using the program PLATON.[40]

3.5. Powder X-ray diffractometry (XRPD). As shown in Figure 10, the experimental powder patterns of the three polymorphs are consistent with the corresponding diagrams calculated from the crystal structure. The most striking joint feature in the X-ray powder patterns is the strongest reflection at about 7.8 ° 2θ ($d \sim 11.3$ Å). The diffractograms allow a clear distinction between mod II° and the two other forms but show a strong similarity between mod I and mod III. This similarity becomes clear from the single crystal structure analysis. The transition of form II° to form I at 140 °C as well as the reversible transformation between mod I and III around −30 °C was confirmed by variable-temperature XRPD. It should be stressed that the PDF-2 database (ICDD, 2006) lists a pattern for OBPHC, which can be clearly identified as the high-temperature form I. According to the original paper,[34] the form was recorded without pretreatment as obtained from the manufacturer. Thus, both polymorphs, form II° as well as form I, may be present in commercial batches of OBPHC.

3.6. Crystal Structure Analysis. The crystal data of the different modifications are summarized in Table 1. The OBPHC molecules adopt essentially two types of conformations in the different polymorphs, a linear (type I) and a bent type (type U) (Figure 11), leading to different packing modes (Figure 12).

The high flexibility of the molecule is reduced by an intramolecular hydrogen bond ($NH_2\cdots O$, Table 3) and intramolecular interactions of the phenyl hydrogens (C6−H6, C2−H2) with the oxygen atoms O2 and O3. Thus, the atoms O1, N1, C11, O2, and O3 form a rigid plane motif with the phenyl ring in all three modifications and all conformers. Figure 11 shows the two types of molecular conformations, each along two axes. This planar structure unit allows a 180° rotation around the C4–C11 bond, maintaining the same interactions as before. As illustrated in the packing diagrams in Figure 12, the molecules form chains that are linked by $NH_2\cdots Cl^-$ and $N^+H\cdots Cl^-$ interactions.

The six torsion angles labeled in the Table 4 as $\tau1$, $\tau2$, $\tau3$, $\tau4$, $\tau5$, and $\tau6$, indicate the areas with significant differences between the different polymorphs. The torsional difference between the three modifications occurs because of the flip in the methyl carbons of the diethylamino ethyl groups of the oxybuprocaine cation. The torsion angles $\tau1$ and $\tau2$ are unusual in that the substituents at the C13−NH bond are distorted in position from those of the normal staggered situation, with torsion angles of ca. 108°, 126° in U1, ca. 102°, 134° in U2, and ca. 149°, 83° in U3 and 66°, 167° in U4 from C-12 to the two ethylamine methylene carbons. Moreover, the carbonyl bond is nearly trans to the C-12 to C-13 bond for molecule U1, U2, U3, and U4 but essentially eclipses one of the CH_2 hydrogens for the I molecule. Such conformations are relatively rare; a search of the Cambridge Structure Database (CSD)[35] produced 67 hits with fragments similar to the diethylamino side-chain of OBPHC, but only one entry (code NANFOY) contains an essentially eclipsed conformation, whereas the other 66 have essentially staggered conformations.

Mod I crystallizes in the monoclinic space group *I*2/*a* with one molecule of conformation U1 in the asymmetric unit. In the crystal structure, the cations and anions are interlinked in a head-to-tail fashion forming zigzag chains of $NH_2\cdots Cl^-$ and $N^+H\cdots Cl^-$ interactions along the *b*-axis. The second hydrogen atom of the amino group interacts with an oxygen atom of the *n*-butoxy chain through an intramolecular $NH_2\cdots O$ contact, and a third contact is formed between the protonated tertiary nitrogen atom and a second chloride, as depicted in Figure 13. Furthermore, a short linear $CH\cdots Cl^-$ bridge between the terminal alkyl (14)CH and chloride with an interatomic distance of 2.64 Å (θ 178°) provides additional stability to these chains, forming a 2D network structure. Interestingly, the terminal alkyl groups (C9−C10, C14−C15, C16−C17) of the cations in two successive chains along the *a*-axis merely contribute to the close packing. In contrast, mod II° crystallizes with two independent molecules of different conformations (I and U2) in the monoclinic space group $P2_1/n$ with a similar arrangement involving two $NH_2\cdots Cl^-$, two $N^+H\cdots Cl^-$, and three weak $CH\cdots Cl^-$ bridges leading to zigzag chains of double the order when compared to mod I along the *a*-axis (Figure 14). In contrast to mod I, the two successive inversion-related chains along the *b*-axis are interlinked by a short $CH\cdots O$ interaction (*d* 2.16 Å, θ 163°), forming the mode of association between the layers. The I-type conformation is unusual in that there are many *gauche* relationships in the (diethylamino)ethyl ester side-chain, which results in significant carbon-13 chemical shifts, as described above. Mod III adopts the monoclinic space group $P2_1/a$ with two conformationally different molecules U3 and U4. The crystal packing shows shifted chains of two different type U molecules, i.e., the two conformers U3 and U4 form a separate zigzag chains involving $NH_2\cdots Cl^-$ and $N^+H\cdots Cl^-$ interactions (Figure 15, Table 3). Additionally, the structure of mod III exhibits a greater variety of short intra- and intermolecular contacts, including short stacking $\pi\cdots\pi$ and $C-H\cdots O$ interactions.

Analysis of modifications I–III shows that there are close similarities in terms of molecular packing. First, in the packing arrangement of all three modifications the dominant structural feature is a zigzag chain of molecules linked by $NH_2\cdots Cl^-$ and $N^+H\cdots Cl^-$ interactions (Figure 12−Figure 15, Table 3). In mod II° both types of conformations (U and I) could be found, whereas in mod I and III only the type U molecule is present in the asymmetric unit. Because of the mixture of molecule types U (**U2**) and I present in modification II, the chain is assembled by an alternating order of the two types, and the size is doubled in comparison to modification I (Figure 12). However, in mod III two different sorts of the type U (U3 and U4) exist each

Table 4. Torsion Angles, τ1, τ3, τ3, τ4, τ5, and τ6, Corresponding to Methyl Carbons of the Diethylamino Ethyl Groups in Different Polymorphs of Oxybuprocaine Hydrochloride

crystal form	τ1 (°) C12−C13−N2−C14	τ2 (°) C12−C13−N2−C16	τ3 (°) C15−C14−N2−C13	τ4 (°) C15−C14−N2−C16	τ5 (°) C17−C16−N2−C13	τ6 (°) C17−C16−N2−C14
			Mod I			
U1	−108.1	125.7	175.5	−58.7	−59.7	−173.6
			Mod II°			
I	58.8	−172.4	67.4	−59.8	171.4	−59.7
U2	102.0	−134.2	−171.8	63.8	70.8	−167.0
			Mod III			
U3	−148.6	83.1	75.2	−156.0	−56.3	73.4
U4	66.4	−166.7	67.7	−168.6	180.0	56.7

Table 5. Physicochemical Data of OBPHC Crystal Forms[a]

modification	mod I	mod II°	mod III
production	cryst from methanol, acetone, ethylacetate heating II° > 140 °C	commercial product, cryst from ether/ethanol	cooling mod I below −33 °C
melting point (°C)	159.9 ± 0.1	<I	<I (∼156 calc)
enthalpy of fusion (kJ·mol^{-1} ± 95% c.i.)	35.5 ± 0.4	∼41 (calc)	∼36 (calc)
experimental transition temperature (°C)	−35 (I → III)	135 (II° → I)	−31 (III → I)
enthalpy of transition (kJ·mol^{-1} ± 95% c.i.)	−0.4 ± 0.1 (I → III)	+5.4 ± 0.1 (II° → I)	+0.4 ± 0.2 (III → I)
thermodynamic transition temperature (°C)	−33 ± 2 (I ↔ III)	∼90 (II° ↔ I)	−33 ± 2 (I ↔ III)
IR data (cm^{-1})	at 25 °C	at 25 °C	at −40 °C
ν N−H (IR)	3465	3469	3467
ν C═O (IR/Raman)	1706/1701	1708/1705	1705/1696
ν C−O−C (IR/Raman)	1265/1258	1259/1256	1271/1262
density (g cm^{-1})			
measured (25 °C)	1.171 ± 0.001	1.180 ± 0.002	
calculated (from single crystal data (at °C)	1.171 (20)	1.183 (20)	
		1.204 (−73)	1.231 (−73)
order of stability at 20 °C	2	1	3

[a] Cryst.: crystallized; calc.: calculated value; c.i: confidence interval.

forming a separate zigzag chain. The differences between modifications I and III lie in the orientation of the terminal alkyl groups (C9−C10, C14−C15, C16−C17). The angle between the linear parts of the zigzag motif is around 120° in all three modifications. The stacking interactions in mod I and mod II° are, however, weak. All in all, a great variety of short intra- and intermolecular contacts, including $\pi\cdots\pi$ and C−H···O interactions, stabilize modifications I–III.

3.7. Conformational Energies. To estimate which of the conformer types (U or I) is lower in energy, the relative potential energies for the 14 starting geometries (i.e., taken from the crystal structures) were calculated and are given in the Supporting Information. Geometries of the energy-minimized structures were in general all very similar to the starting geometry taken from the crystal structure, with the exception of some variation in torsion angles, especially C12−C13−N2−C14. This may be because the chloride ion, which forms a hydrogen bond to the protonated diethylamine group (the proton was also excluded), may hold this torsion angle in a higher-energy conformation.

The value of the torsion angles C2−C3−O1−C7, C3−O1−C7−C8, and C1−C11−O3−C12 are the same in both the I and the U conformations. The difference between the I and U conformers is in the torsion angle C2−C1−C11−O3. Conformations that differ in the arrangement of the *n*-butoxy chain, from all torsion angle being *anti* to the presence of one being *gauche* (O1−C7−C8−C9) raises the energy of the conformer by about 1–2 kJ mol^{-1}. The major difference between the U conformers in mod I and mod III is the rotation of the torsion C7−C8−C9−C10 from *anti* in the room tempertaure form (around 180°) to *gauche* (around 60°) in the low temperature form (mod III).

In general, the energy in the gas phase of the I conformer is predicted by MMFF to be between 6 and 12 kJ mol^{-1} lower in energy than the U conformer. So the molecular mechanics suggests that only the stable crystal structure of OBPHC (mod II°) contains the most stable conformer together with a less stable one.

The stochastic conformational search predicted the I-conformation found in the crystal structure to be within 1.2 kJ mol^{-1} of the global minimum. The coordinates of the 14 energy-minimized structures discussed previously, and geometry of the lowest energy conformer found with the stochastic search are given in the Supporting Information.[36,37]

3.8. Thermodynamic and Kinetic Stability of the Polymorphs. Table 5 summarizes the most important thermodynamic data of the modifications as well as the densities and the wavenumbers of some IR/Raman modes, and the scheme in Figure 16 illustrates the production and transformation pathways. The fact that the melting points and enthalpies of fusion of mods II° and III cannot be determined makes the determination of the relative thermodynamic relationship of the polymorphs and the construction of a semischematic energy temperature diagram[16,38,39] (Figure 17) difficult. However, from the measured transitions (endothermic transition of II° to I and the reversible transition between III and I), considering the heat of transition rule,[16] we can clearly conclude that mod I is enantiotropically related to both mod II° and mod III. In that

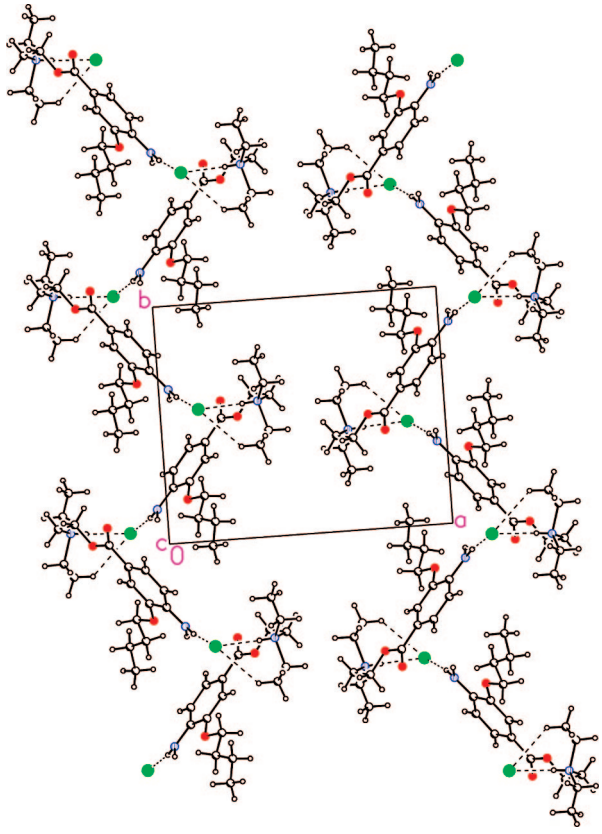

Figure 13. Crystal packing of mod I showing zigzag chains of $NH_2\cdots Cl^-$ and $N^+H\cdots Cl^-$ interactions involving the screw related molecules along *b*-axis running in opposite directions.

the enthalpy of transition of II° to I is significantly higher than that of the pair III and I, we can furthermore conclude that the enthalpy curve of mod III runs below that of mod I, but above the enthalpy curve of mod II°. This allows us to fix the free energy order at 0 K to II° < III < I. confirming that mod II° shows the highest stability followed by mod III and I at absolute zero temperature. Since mod II° and mod III are enantiotropically related to mod I, their free energy curves must intersect with the free energy curve of mod I below their melting temperature, which makes it obvious that the melting points of II° and III are both lower than the melting point of mod I (see Figure 17).

Whether the virtual melting point of mod II° is higher or lower than that of mod III is ambiguous. Since we could not observe an interconversion between these two forms, the relationship can only be estimated from the course of the free enthalpy curves and calculations utilizing the obtained thermochemical data, which are however very prone to errors and allow only rough estimations. Our data allow us to conclude that mod III is less stable than form II° below the transition temperature II°/I as becomes also obvious from the course of the G curves in Figure 17. This transition occurs in DSC experiments at about 135 °C, but, as expected, from solvent-mediated transformation studies in toluene we know that the thermodynamic transition temperature II°/I is lower, namely, close to 90 °C. This is also confirmed by the temperature controlled FTIR experiments, where the transition of mod II° to mod I in a KBr pellet occurred already at about 100 °C. It is possible that the free energy curves of mod II° and mod III intersect (enantiotropism) in the temperature range of about 110 and 150 °C, but it is also possible that they do not intersect below their melting points (monotropism). Calculations based on the melting data of mod I,

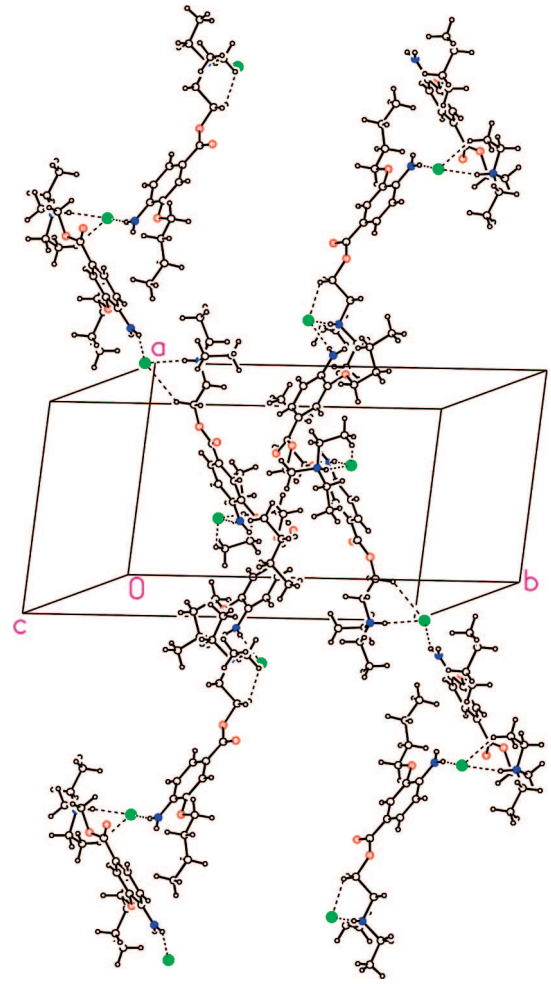

Figure 14. Crystal packing of mod II° showing $NH_2\cdots Cl^-$ and $N^+H\cdots Cl^-$ hydrogen bonded chains along *a*-axis running in opposite directions.

the measured transition enthalpies and the transition points indicate an enantiotropic relationship and result in melting points of ~156 (mod III) and ~150 °C (mod II°). However, such calculations require the knowledge of precise melting enthalpies, which, in case of forms II° and III, have been just roughly estimated from the differences between experimentally determined enthalpy data ($\Delta_{fus}H_I$ and the transition enthalpies $\Delta_{trs}H_{III\text{-}I}$, $\Delta_{trs}H_{I\text{-}III}$, see Table 5) without considering the heat capacities differences of the solid phases and the temperature differences of the phase transitions. Therefore, even a small error in the experimental data can result in the wrong conclusion, so we have to confess that the thermodynamic relationship between mod II° and mod III is not clear from the available data. Anyway, it is clear that mod II° is the thermodynamically stable polymorph below about 90 °C and mod I above this temperature, whereas mod III is metastable in the entire temperature range. It is remarkable that none of the produced samples of mod I, regardless whether they were obtained by crystallization or from the melt, transformed to mod II° within several years of storage in glass vials. This displays its extraordinary high kinetic stability at ambient conditions. Therefore, it is not surprising that either mod I or mod II° can be found in commercial samples and that solid-state reference data of the substance may be inconsistent. The fact that the pattern of mod I is filed in the powder diffraction file of the ICDD confirms this statement.

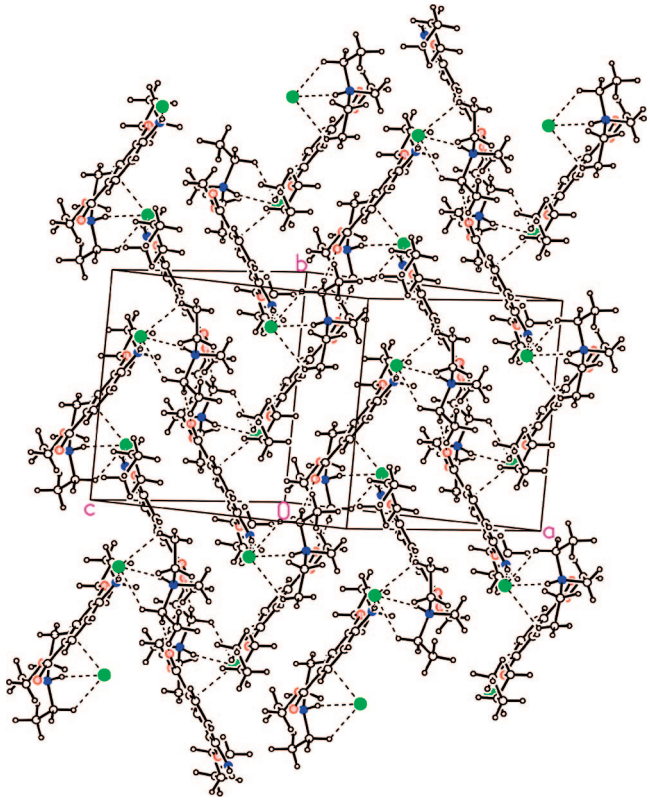

Figure 15. Crystal packing of mod III showing the herringbone packing arrangement. $NH_2\cdots Cl^-$, $N^+H\cdots Cl^-$, and $CH\cdots Cl^-$ interactions are shown as dotted lines.

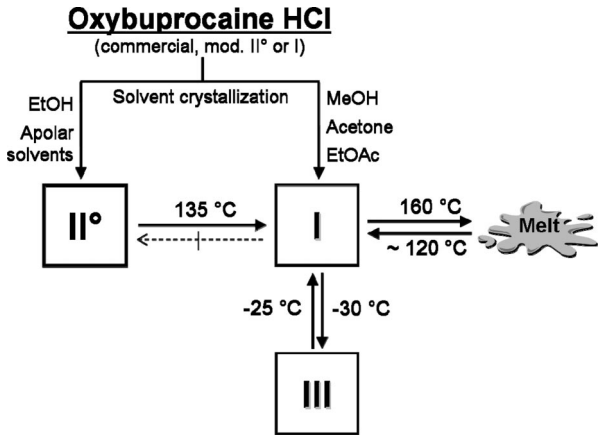

Figure 16. Scheme illustrating the production and transformation pathways between the oxybuprocaine hydrochloride polymorphs.

Finally, it should be mentioned that in case of the pair II°/III, we are faced with a further exception to the density rule.[16] The difference of 2.2% (calculated densities at 200 K, see Table 5) is significant and confirms the high incidence of such exceptions in polymorphic pairs of conformational flexible molecules, which may provide differently shaped "building blocks" as it is the case here (U + I type conformations in mod II°, two U type conformers in mod III).

4. Conclusions

OBPHC is an intriguing example of conformational polymorphism displaying a complexity of molecular arrangements of compounds with a high conformational flexibility. Though a

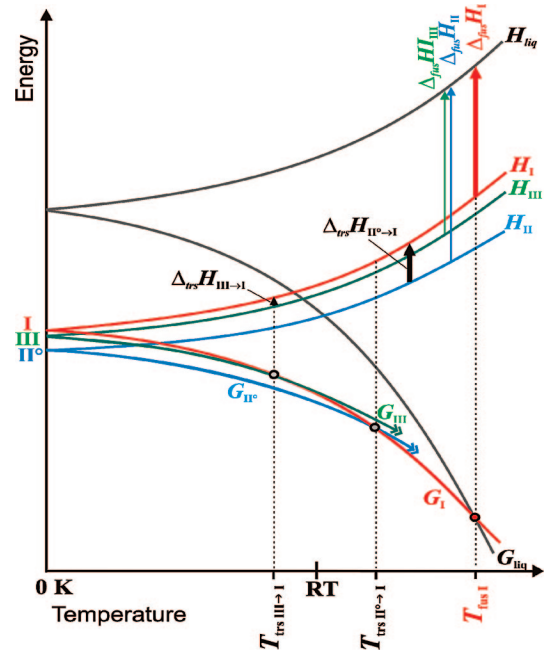

Figure 17. Semischematic energy-temperature diagram of oxybuprocaine hydrochloride polymorphs. *G*: free enthalpy curves, *H*: enthalpy curves of the melt (liq), mod I, mod II°, and mod III; T_{trs}: thermodynamic transition point; $\Delta_{fus}H$: enthalpy of fusion; T_{fus}: melting point; thick arrows between the enthalpy curves mark measured values.

variety of conformations is theoretically possible, only two basic types of conformation (U and I) can be found in the three crystal forms. It is worth mentioning that the most stable I-conformer is only present in mod II°, the thermodynamically stable form below temperatures of about 90 °C. However, this modification contains also a less stable U-conformer, which confirms that a stable polymorph can also consist of energetically less favorable conformations.

The polymorphs show different intermolecular hydrogen bonds, but the bond lengths in mods I and II° are very similar. Therefore, the band shifts of the vibrational spectra and changes in ^{13}C NMR chemical shifts of mods I and II° are probably caused mainly by the differences in dihedral angles of the side-chains. The dipolar dephasing experiments and the variable-temperature NMR spectra give evidence of substantial mobility toward the end of the side-chains. NMR also provides evidence of the number of molecules in the asymmetric units and of the strengths of the hydrogen bonds.

The thermodynamically stable form mod II° is commonly present in commercial products. Mod I, the high-temperature form, is characterized by a high kinetic stability. A transformation to the stable mod II° only proceeds in a solvent-mediated process but not in the solid state. Instead, mod I shows a spontaneous and highly reversible transformation to a third form (mod III) at −33 °C. Similar reversible low-temperature transitions showing significant conformational changes of flexible molecular moieties but rather subtle changes in the overall crystal packing have been also encountered in the polymorphic monohydrates of the 1:1 molecular complex (cocrystal) of tetroxoprim-sulfametrol[41] or in polymorphs of pramocaine base and hydrochloride.[42] Crystallization from solvents results either in the stable mod II°, the metastable mod I or mixtures of these forms, whereas in the crystallization from the melt only mod I is obtained. Therefore, mod I may also be present in commercial products. However, due to its high kinetic stability, this

metastable form is also qualified for the production of solid drug formulations.

Acknowledgment. We thank A. Schmidt and Ing. E. Gstrein (University of Innsbruck, Institute of Pharmacy) for experimental contributions. One of us (R.K.H.) is grateful to the Leverhulme Trust for the provision of an Emeritus Fellowship. We also thank the U.K. EPSRC for financial support under grants GR/N05635 and GR/R81466. We are grateful to P. Y. Ghi for assistance with some NMR spectra. R.K.R.J. acknowledges financial support from a Lise-Meitner grant M862-B10 of the FWF (Austrian Science Fund).

Supporting Information Available: Microphotographs of OBPHC mod II° before and after transformation to mod I, photographs of single crystals of mods I and II°, Dipolar-dephased (NQS) spectrum of mod I, series of temperature-controlled solid-state ^{13}C NMR spectra of OBPHC mod I at and below ambient temperature, overlay plots of the different molecular conformations, thermal ellipsoid plots of the different conformations in the three polymorphs, a plot of the disorder of the side-chains in modifications I and II, and a table with the relative energies of minimized conformations with selected torsion angles. This information is available free of charge via the Internet at http://pubs.acs.org.

References

(1) Grant, D. J. W. In *Polymorphism in Pharmaceutical Solids*; Brittain, H. G., Ed.; Marcel Dekker, New York, 1999; pp 1–33.
(2) Bernstein, J.; Hagler, A. T. *J. Am. Chem. Soc.* **1978**, *100*, 673–681.
(3) Bernstein, J. Conformational Polymorphism. In *Organic Solid State Chemistry*; Desiraju, G. R., Ed.; Esevier: Amsterdam, 1987; pp 471–518.
(4) Bernstein, J. *Polymorphism in Molecular Crystals*;Clarendon Press: Oxford, 2002.
(5) Davey, R. J.; Blagden, N.; Potts, G. D.; Docherty, R. *J. Am. Chem. Soc.* **1997**, *119* (7), 1767–1772.
(6) Yu, L.; Stephenson, G. A.; Mitchell, C. A.; Bunnell, C. A.; Snorek, S. V.; Bowyer, J. J.; Borchardt, T. B.; Stowell, J. G.; Byrn, S. R. *J. Am. Chem. Soc.* **2000**, *122* (4), 585–591.
(7) Gerber, J. J.; Caira, M. R.; Lötter, A. P. *J. Cryst. Spectrosc. Res.* **1993**, *23*, 863–869.
(8) Vega, D. R.; Polla, G.; Martinez, A.; Mendioroz, E.; Reinoso, M. *Int. J. Pharm.* **2007**, *328* (2), 112–118.
(9) Schouten, A.; Kanters, J. A.; Kroon, J.; Comini, S.; Looten, P.; Mathlouthi, M. *Carbohydr. Res.* **1998**, *312* (3), 131–137.
(10) Starbuck, J.; Docherty, R.; Charlton, M. H.; Buttar, D. *Journal of the Chemical Society-Perkin Transactions II* **1999**, (4), 677–691.
(11) Bar, I.; X *J. Pharm. Sci.* **1985**, *74*, 255–263.
(12) He, X.; Griesser, U. J.; Stowell, J. G.; Borchardt, T. B.; Byrn, S. R. *J. Pharm. Sci.* **2001**, *90* (3), 371–388.
(13) Schottenberger, H.; Wurst, K.; Griesser, U. J.; Jetti, R. K. R.; Laus, G.; Herber, R. H.; Nowik, I. *J. Am. Chem. Soc.* **2005**, *127* (18), 6795–6801.
(14) Yu, L.; Reutzel-Edens, S. M.; Mitchell, C. A. *Org. Process Res. Dev.* **2000**, *4* (5), 396–402.
(15) Bauer, J.; Spanton, S.; Henry, R.; Quick, J.; Dziki, W.; Porter, W.; Morris, K. *Pharm. Res.* **2001**, *18* (6), 859–866.
(16) Burger, A.; Ramberger, R. *Mikrochim. Acta* **1979**, *II*, 259–271.
(17) Kitaigorodsky, A. I. *Molecular Crystals and Molecules*; Academic Press: New York, London, 1973.
(18) Chen, X.; Morris, K. R.; Griesser, U. J.; Byrn, S. R.; Stowell, J. G. *J. Am. Chem. Soc.* **2002**, *124* (50), 15012–15019.
(19) Day, G. M.; Motherwell, W. D. S.; Ammon, H. L.; Boerrigter, S. X. M.; la Valle, R. G.; Venuti, E.; Dzyabchenko, A.; Dunitz, J. D.; Schweizer, B.; van Eijck, B. P.; Erk, P.; Facelli, J. C.; Bazterra, V. E.; Ferraro, M. B.; Hofmann, D. W. M.; Leusen, F. J. J.; Liang, C.; Pantelides, C. C.; Karamertzanis, P. G.; Price, S. L.; Lewis, T. C.; Nowell, H.; Torrisi, A.; Scheraga, H. A.; Arnautova, Y. A.; Schmidt, M. U.; Verwer, P. *Acta Crystallographica, Section B: Structural Science* **2005**, *B61* (5), 511–527.
(20) Gavezzotti, A. *Crystallography Reviews* **1998**, *7*, 5–121.
(21) Lewis, T. C.; Tocher, D. A.; Price, S. L. *Crystal Growth & Design* **2004**, *4* (5), 979–987.
(22) Griesser, U. J.; Auer, M. E.; Burger, A. *Microchem. J.* **2000**, *65* (3), 283–292.
(23) Griesser, U. J.; Auer, M. E.; Burger, A. *Sci. Pharm.* **1999**, *67*, 319–330.
(24) Harris, R. K.; Cadars, S.; Emsley, L.; Yates, J. R.; Pickard, C. J.; Jetti, R. K. R.; Griesser, U. J. *Phys. Chem. Chem. Phys.* **2007**, *9* (3), 360–368.
(25) Harris, R. K. *The Analyst* **2006**, *131*, 351.
(26) Opella, S. J.; Frey, M. H. *J. Am. Chem. Soc.* **1979**, *101*, 5854–5856.
(27) Kraus, W.; Nolze. G. *PowderCell for Windows,* version 2.3; Bundesanstalt fuer Materialforschung und-pruefung Berlin, Germany, 1995.
(28) Altomare, A.; Cascarano, G.; Giacovazzo, C.; Guagliardi, A. *J. Appl. Crystallogr.* **1993**, *26*, 7–13.
(29) *SHELXTL,* version *Version 6.12.*; Bruker AXS Inc.: Madison, WI, USA, 2000.
(30) *Maestro Molecular Modeling Interface,* version 7.5; Schrödinger: LLC, 2006.
(31) *MOE,* version 2007.07; Chemical Computing Group: 2007
(32) Fukuoka, E.; Makita, M.; Yamamura, S. *Chem. Pharm. Bull.* **1989**, *37* (4), 1047–1050.
(33) Kerc, J.; Srcic, S. *Thermochim. Acta* **1995**, *248* (JAN), 81–95.
(34) Koundourellis, J. E.; Malliou, E. T.; Sullivan, R. A. L.; Chapman, B. *Journal of Chemical & Engineering Data* **2000**, *45* (6), 1001–1006.
(35) (a) Allen, F. H. *Acta Crystallogr B,* **2002**, *58*, 380–388. (b) The CSD search was performed using Conquest version 1.8 (CSD 5.27, Nov. 2005,353 518 entries) with the following filters used: 3D coordinates determined, and only organics.
(36) Halgren, T. A. *J. Comput. Chem.* **1999**, *20* (7), 730–748.
(37) Ercanli, T.; Boyd, D. B. *J. Chem. Inf. Model.* **2005**, *45* (3), 591–601.
(38) Grunenberg, A.; Henck, J.-O.; Siesler, H. W. *Int. J. Pharm.* **1996**, *129*, 147–158.
(39) Yu, L. *J. Pharm. Sci.* **1995**, *84*, 966–974.
(40) PLATON, Version 1.08, 2005 Spek, A. L. *J. Appl. Crystallogr.* **2003**, *36*, 7–13.
(41) Caira, M. R.; Bettinetti, G.; Sorrenti, M.; Catenacci, L. *J. Pharm. Sci.* **2003**, *92* (11), 2164–2176.
(42) Schmidt, A. C.; Senfter, N.; Griesser, U. J. *J. Therm. Anal. Calorim.* **2003**, *73* (2), 397–408.

CG070590D